



# Vibration mode localization in single- and multi-layered graphene nanoribbons



Deepti Verma <sup>a</sup>, S.S. Gupta <sup>b,\*</sup>, R.C. Batra <sup>c</sup>

<sup>a</sup> Department of Materials Science and Engineering, IIT Kanpur, Kanpur 208016, India

<sup>b</sup> Mechanics and Applied Mathematics Group, Department of Mechanical Engineering, IIT Kanpur, Kanpur 208016, India

<sup>c</sup> Department of Engineering Science and Mechanics, M/C 0219, Virginia Polytechnic Institute and State University, Blacksburg, VA 24061, USA

## ARTICLE INFO

### Article history:

Received 24 March 2014

Received in revised form 28 June 2014

Accepted 2 July 2014

### Keywords:

Graphene nanoribbons

Vibrations

Mode localization

Molecular mechanics

Continuum mechanics

## ABSTRACT

We study vibrations of single- and multi-layered rectangular graphene nanoribbons (GNRs) using molecular mechanics (MM) simulations by employing the MM3 potential. Two sets of boundary conditions are considered, namely, clamping atoms on either all four edges (CCCC) or on the two small edges (CFCF). Furthermore, we consider two scenarios for a single-layered GNR – one in which an interior atom is held stationary and the other in which a bucky-ball is covalently bonded to an interior atom. For multi-layered GNRs an interior atom only on the outermost layer is either held fixed or has a bucky-ball covalently bonded to it. For CCCC single- and multi-layered GNRs, both scenarios are found to divide the GNR into two differently vibrating regions such that in one region atoms have negligible while in the other region large out-of-plane displacements; we call this *mode localization*. For multi-layered GNRs, mode localization in the outermost layer leads to *cooperative mode localization* in the remaining layers. We also study vibrations of prestretched CFCF single-layered GNRs with and without a covalently bonded bucky-ball, and find that the attached bucky-ball localizes modes in a certain region of the single-layered GNRs. For an unstretched single-layered GNR a very interesting result from MM simulations is that one region undergoes bending while the other torsional vibration. The results for single-layered GNRs with CFCF boundary condition are correlated with those derived from continuum models, namely a stretched string-mass and a Kirchhoff plate. The frequency equation for the string-mass model is derived by solving the equation of motion using the Laplace transform technique. Frequencies of vibrations of the Kirchhoff plate are numerically found by using the finite element method. With increasing value of the prestretch the string-mass system is found to have bending mode frequencies that are closer to those of the CFCF single-layered GNR than those of the Kirchhoff plate. Using potential energy of deformation at each atom, for multi-layered GNRs with a fixed interior atom, and for single-layered GNRs with a covalently bonded bucky-ball, it is found that the classical parameter for quantifying vibration mode localization is not valid; hence a new parameter is defined. This work highlights the importance of modes of vibration for designing sensors to detect a mass attached to either a single- or a multi-layered GNR.

© 2014 Elsevier B.V. All rights reserved.

## 1. Introduction

Single- and multi-layered graphene sheets (S/MLGSs) and graphene nanoribbons (GNRs) have been studied using either molecular mechanics/dynamics (MM/MD) simulations [1–6] or experimentally as nano-electro-mechanical-systems (NEMSs) actuators and sensors [7–12]. In order to quickly realize a workable and reliable system, an accurate knowledge of dynamic characteristics of S/MLGSs and GNRs is needed. Furthermore, some researchers have analyzed dynamic/static deformations of S/MLGSs and GNRs

to find their elastic constants and basal plane stiffness [2,10]. To achieve these objectives one usually compares dynamic/static characteristics of graphene sheets (GSs) and nanoribbons (NRs) with those of their equivalent continuum structures (ECSs). In the studies listed above these ECSs are considered to be either thin beams/plates/strips or membranes. For an MLGS or a multi-layered GNR the ECS could be a thin plate/membrane (equal to the number of layers in the MLGS or multi-layered GNR) interconnected with each other through van der Waals springs [13,14].

In NEMSs, atoms on the edges of an S/MLGS or a GNR are invariably attached to a substrate and the interaction between them may be due to van der Waals forces [7,10,12]. Modelling such interactions, which translate as boundary conditions for the ECS, is

\* Corresponding author.

E-mail address: [ssgupta@iitk.ac.in](mailto:ssgupta@iitk.ac.in) (S.S. Gupta).

computationally very challenging. Approximating these interactions as clamped/simply supported or compliant boundary conditions (if the substrate is taken as flexible) on the edges of the ECS can lead to a wide variation in results [7,10]. In most cases it is found that an ECS in the form of a thin plate/membrane predicts well the vibrational characteristics and the basal plane stiffness of GSs and NRs.

Filоче and Mayboroda [15] recently showed that if a thin elastic rectangular Kirchhoff plate clamped on all edges has an interior point held stationary then a line through that point in the plane of the plate and parallel to an edge of the plate divides it into two independently vibrating regions. Thus, at a given frequency the corresponding standing wave will have almost negligible amplitude in a region. Filоче and Mayboroda [15] termed this phenomenon *mode localization*. Furthermore, they showed that with an increase in the aspect ratio of plates the localization of modes in one of the two regions increased. In a similar study, Sharma et al. [16] showed that for thin elastic orthotropic Mindlin plates one can tailor either the material properties or the lamination scheme to exploit the phenomenon of mode localization for controlling vibration/noise. They also found that adding a mass at an interior point of a plate localizes modes.

We envisage two situations similar to those studied in [15,16] for S/MLGSs and GNRs: (i) a single- or multi-layered GNR is kept over a patterned surface etched in a trench, and (ii) a single- or multi-layered GNR is used as a mass sensor that attracts a single foreign atom. In the first scenario the single- or multi-layered GNR placed over a trench may have an interior atom interacting with an etched pillar of height greater than that of other pillars in the trench in such a way that the atom of the single- or multi-layered GNR is considered to be fixed to that pillar. And, in the second case a molecule is bonded covalently or attached by van der Waals force to an interior atom. The second scenario is more commonly encountered. A typical GNR based mass sensor is functionalized with receptors such that it adsorbs/attracts a single molecule with greater probability. Hence, it is likely that when such a sensor adsorbs/attracts a foreign molecule it will exhibit mode localization due to mass loading because a GNR behaves like a thin plate/membrane. This localization in turn may impair the measurement of the out-of-plane vibrations depending on which side of the GNR is probed. Hence, one may need to amplify and filter the signal to increase the signal to noise ratio. This will require additional electronics which may lead to a bulky and un-manageable sensor system. As far as we know there is no available work in the open literature that elucidates this phenomenon for a graphene based mass sensor. A prior knowledge of *mode localization* while designing a *sensitive mass sensor* may provide useful guidelines on the placement of probes.

The rest of the paper is organized as follows. In Section 2 we describe the MM simulations using the MM3 potential. The mode localization in single- and multi-layered GNRs due to fixing an interior atom is studied in Section 3 where we also explain the cooperative mode localization for multi-layered GNRs. In Section 4 the mode localization in single- or multi-layered GNRs due to an attached foreign molecule and its quantification is discussed. We

correlate results from MM simulations with those from continuum theories in Section 5. Conclusions of this work are summarized in Section 6.

## 2. Molecular mechanics simulations

We consider rectangular single- and multi-layered GNRs with two different boundary conditions on its edges. In one case all atoms on the four edges are fixed and in the other, atoms only on two short edges are fixed; the former is usually called clamped–clamped clamped–clamped (CCCC) and the latter clamped–free–clamped–free (CFCF) boundary condition. Fixing or clamping an atom implies that its three translational displacements are equal to zero. Furthermore, the mode localization in these ribbons is studied due to either fixing an interior carbon atom or covalently bonding a bucky-ball to an interior carbon atom of a single-layered GNR (in case of a multi-layered GNR an atom on its outermost layer). The NRs without an interior fixed atom and carrying no bucky-ball will be referred to as *pristine NRs* and those with one of these conditions as *treated NRs*.

Vibration characteristics of GNRs are studied using molecular mechanics (MM) simulations employing an open source code TINKER [20] and the MM3 [17] potential. We have found the MM3 [17] potential to be appropriate for modelling single-layered GNRs due to the similarity between graphitic bonds in the GNRs and the aromatic protein structures for which the potential was constructed. The mathematical expression of the potential is given by Eq. (1). The terms  $U_s$ ,  $U_\theta$  and  $U_\phi$  are energies due to bond stretching, bending and torsion, respectively,  $U_{vdW}$  represents van der Waals interaction between non-bonded atoms, and  $U_{s\theta}$ ,  $U_{\phi s}$  and  $U_{\theta\theta'}$  represent energies of cross interactions between stretch–bend, torsion–stretch and bend–bend deformations, respectively. The degrees-of-freedom  $r$ ,  $\theta$ ,  $\theta'$  and  $\phi$  stand for stretch, angle bending, out-of-plane bending and dihedral torsion, respectively. A subscript,  $e$ , on a variable signifies its value in the configuration of the global minimum potential energy.

$$U = \sum_i \sum_j (U_s + U_\theta + U_\phi + U_{s\theta} + U_{\phi s} + U_{\theta\theta'}) + \sum_i \sum_k U_{vdW},$$

$$U_s = 71.94K_s(r - r_e)^2 \left[ 1 - 2.55(r - r_e) + \left(\frac{7}{12}\right)(2.55)^2(r - r_e)^2 \right],$$

$$U_\theta = 0.021914K_\theta(\theta - \theta_e)^2 [1 - 0.014(\theta - \theta_e) + 5.6(10)^{-5}(\theta - \theta_e)^2 - 7.0(10)^{-7}(\theta - \theta_e)^3 + 2.2(10)^{-8}(\theta - \theta_e)^4],$$

$$U_\phi = (V_1/2)(1 + \cos \phi) + (V_2/2)(1 - \cos 2\phi) + (V_3/2)(1 + \cos 3\phi),$$

$$U_{s\theta} = 2.51118K_{s\theta} [(r - r_e) + (r' - r'_e)](\theta - \theta_e),$$

$$U_{\phi s} = 11.995(K_{\phi s}/2)(r - r_e)(1 + \cos 3\phi),$$

$$U_{\theta\theta'} = -0.021914K_{\theta\theta'}(\theta - \theta_e)(\theta' - \theta'_e), \text{ and}$$

$$U_{vdW} = \epsilon_e \left\{ -2.25(r_v/r)^6 + 1.84(10)^5 \exp[-12.0(r/r_v)] \right\}. \quad (1)$$

The total potential energy of a body equals the sum of potential energies of all atoms in the body (indices  $i$  and  $j$  in Eq. (1) range over bonded atoms, and the index  $k$  over all atoms). Values of constants

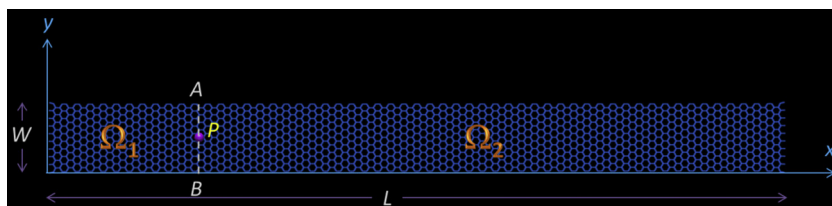
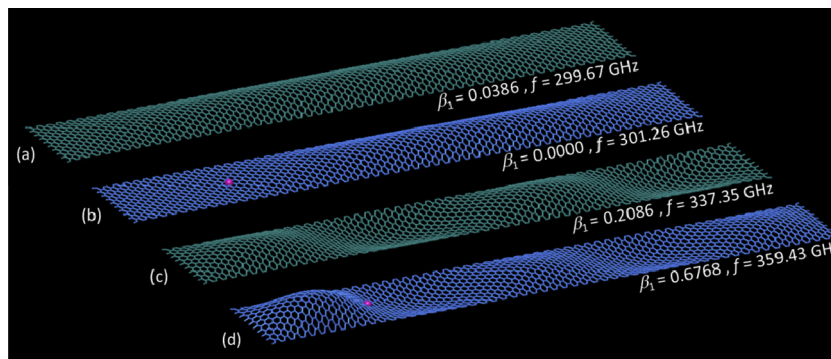


Fig. 1. Structure of a GNR depicting geometric parameters, location of an interior atom at  $P(L/5, W/2)$ , regions  $\Omega_1$  (on the left side of the dividing line  $AB$  passing through  $P$ ) and  $\Omega_2$  (on the right side of the dividing line  $AB$ ) in which vibration modes get localized after fixing an atom or attaching a foreign molecule at  $P$ .



**Fig. 2.** Vibration modes of a single-layered GNR. Modes (1,1) and (4,1) of the pristine GNR are shown in (a) and (c), respectively. Localized (1,1) and (4,1) modes after fixing an interior atom at  $P$ , marked as red dot, are shown in (b) and (d), respectively.

$K_s, K_\theta, V_1, V_2, V_3, \epsilon_e, r_v, K_{s\theta}, K_{\phi s}$  and  $K_{\theta\theta}$  are given in [17,20]. We note that the van der Waals force between two atoms varies as weighted sum of  $(r_v/r)^6$  and  $\exp(-12 r/r_v)$ . The first term is the same as that in the Lennard-Jones potential, but the second term is different. The MM3 potential has been validated by comparing predictions from

it with the test data available in the open literature [10,18] in our previous studies [2,19].

The first step in our work is the minimization of the potential energy of a single- or a multi-layered GNR within rms potential gradient of 0.001 kcal/mol/Å without using a cut-off distance and without applying boundary conditions. For this step MINIMIZE subroutine of TINKER [20] is used. In the second step atoms on the edges are fixed according to the desired boundary conditions and the vibration characteristics of the single- or the multi-layered GNRs are obtained using VIBRATE subroutine. This module computes eigenvalues and eigenvectors of the mass weighted Hessian for the single- or multi-layered GNRs. For a treated GNR in which an interior atom is fixed the procedure is similar to that described above except that besides fixing edge atoms we also fix an interior atom. However, when a foreign molecule is attached to an interior atom of a single-layered GNR, we first compute the minimum potential energy configuration of the bucky-ball alone and then of the system comprised of the equilibrated bucky-ball covalently bonded to the equilibrated clamped pristine GNR, each within rms potential gradient of 0.001 kcal/mol/Å. Subsequently, the vibration characteristics are computed as explained above. Fixing an interior atom and attaching a bucky-ball to an interior atom of a NR leads to localization of modes of vibration. Localization of in-plane and out-of-plane vibration modes (phonons) indicates that the flow of heat

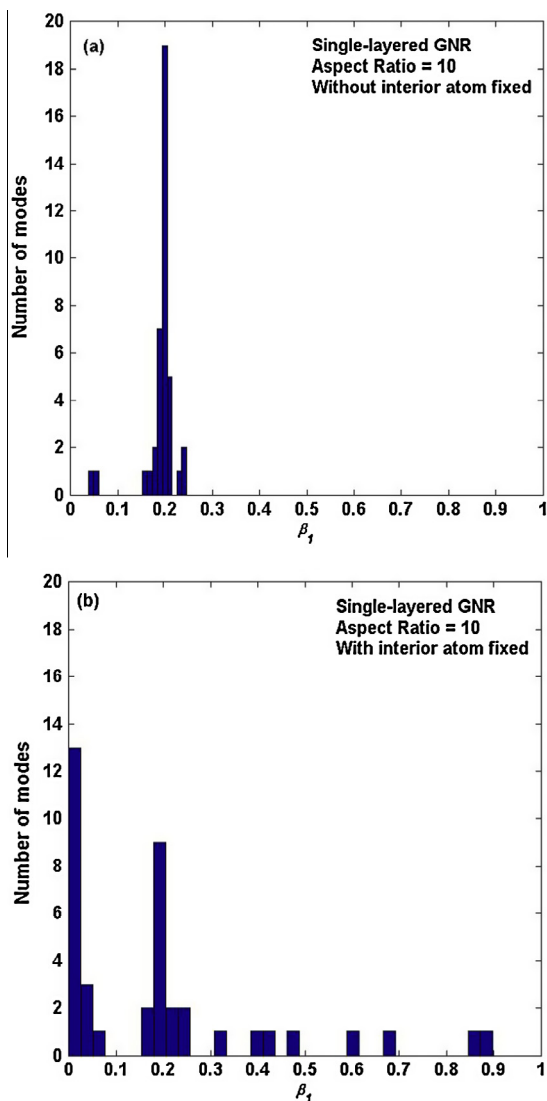


**Fig. 3.** Distribution of the mode localization parameter  $\beta_1$  computed over the first 40 out-of-plane modes for GNR (a) without, and (b) with interior fixed atom at  $P$  (cf. Fig. 1).

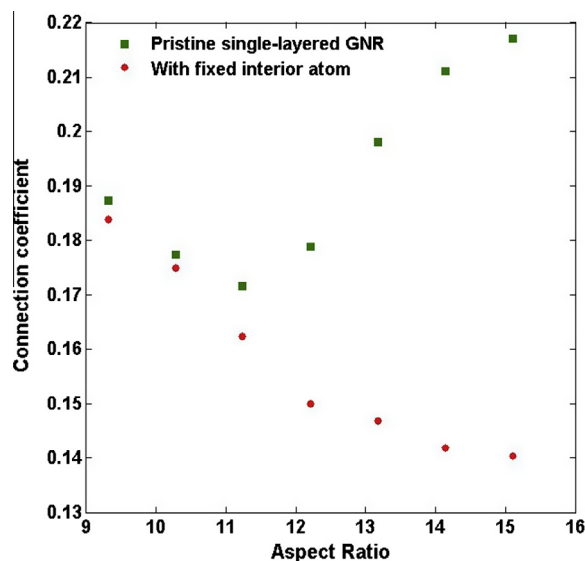


**Fig. 4.** For an atom fixed at  $(L/5, W/2)$  in a CCCC GNR, variation of the connection coefficient with the aspect ratio. We note that the connection coefficient decreases rapidly up to the aspect ratio  $\sim 12$ .

along/across GNRs might be affected. However, in this paper we only study the *out-of-plane* modes of vibration of single- or multi-layered GNRs. Furthermore, we characterize the phenomenon of mode localization by considering first forty out-of-plane modes.

### 3. Mode localization due to fixed interior atom

#### 3.1. Single-layered GNRs

The structure of a single-layered GNR and its geometrical parameters are shown in Fig. 1. The location ( $L/5, W/2$ ) of the fixed

atom is arbitrarily chosen. In mode ( $m, n$ ) the transverse displacement is in the form of  $m$  and  $n$  half sine waves along the  $x$ - and the  $y$ -axes, respectively. The modes (1,1) and (4,1) of a CCCC pristine single-layered GNR are shown in Fig. 2(a) and (c), respectively. In Fig. 2(b) and (d) modes of vibration of the same single-layered GNR after fixing the interior atom are depicted. From the deformed shape shown in Fig. 2(b) it is evident that the out-of-plane displacement of atoms in  $\Omega_1$  is negligible and that in  $\Omega_2$  are of mode (1,1) type. On the contrary, in Fig. 2(d) the out-of-plane displacement of atoms in  $\Omega_2$  is less than that of atoms in  $\Omega_1$  and the mode in  $\Omega_2$  is (4,1) type. Thus, we conceive an imaginary line  $AB$

**Table 1**  
Bending mode (BM) frequencies (in GHz) of one, two, three, four and five-layered GNRs with CCCC boundary condition computed from MM simulations. Dimensions of GNR:  $L = 227.77$  Å and  $W = 20.94$  Å. Number of C-atoms in one layer = 2148. Mode shape corresponding to Mode 1 vibrations of the multi-layered GNRs with a bucky-ball covalently bonded to an interior atom of an outermost layer is shown in Fig. 13.

Structure	No. layers	Mode 1	BM 1	BM 2	BM 3	BM 4
Pristine GNRs	1	–	299.67	306.90	319.56	337.35
	2	–	301.35	308.64	320.97	338.55
	3	–	303.27	310.50	322.74	340.14
	4	–	305.04	312.21	324.33	341.64
	5	–	306.57	313.68	325.74	342.93
GNRs with a fixed interior clamped atom on the outermost layer	1	–	301.26	313.44	333.90	359.43
	2	–	302.91	314.88	334.98	360.18
	3	–	304.59	316.32	336.45	360.93
	4	–	306.51	318.12	337.65	360.78
	5	–	308.01	319.41	338.64	359.79
GNRs with $C_{180}$ attached on an interior atom on the outermost layer	1	179.85	301.50	313.86	334.65	361.89
	2	231.36	308.46	320.64	340.80	378.51
	3	252.12	305.13	317.52	337.74	363.36
	4	275.85	321.27	333.57	353.55	378.63
	5	275.22	308.55	320.85	340.86	365.64

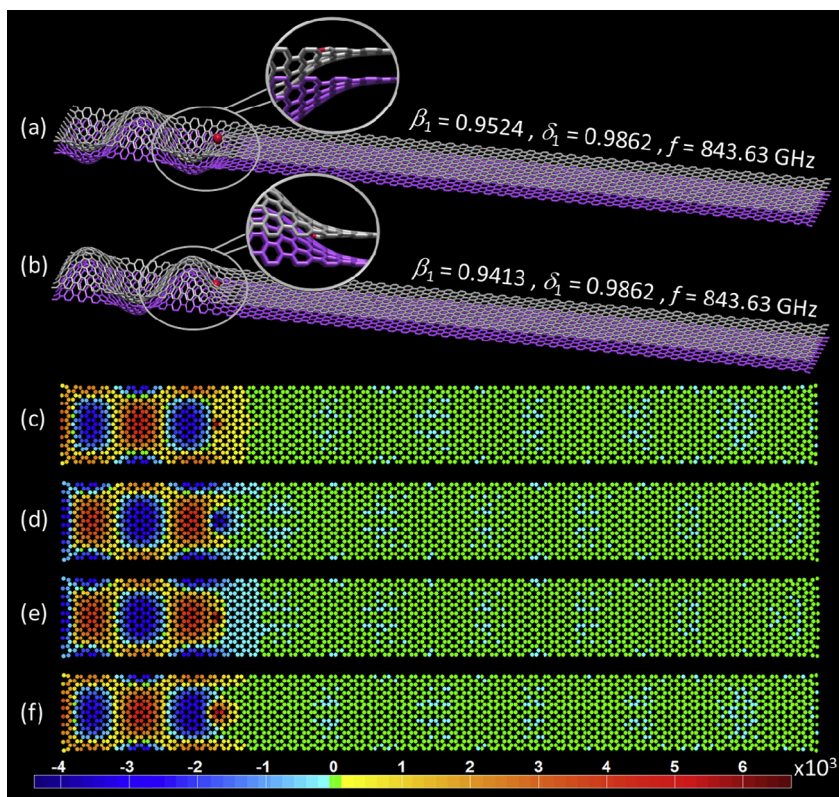


**Fig. 5.** Mode localization in a double-layered GNR when only one layer has a fixed atom (shown in red in a). Deformed shapes (a) and (b) evince asymmetry in the deformation in the two extreme configurations. For one of the extreme positions fringe plots of the potential energy of deformation for the top and the bottom layers are shown in (c) and (d), respectively. Similarly, for the other extreme position fringe plots of the potential energy of deformation for the top and the bottom layers are depicted in (e) and (f), respectively. Fringe plots in (c) through (f) confirm asymmetry in the energy distribution in extreme positions in the top and the bottom layers. The color bar has units of cal/mol. (For interpretation of the references to color in this figure legend, the reader is referred to the web version of this article.)

(cf. Fig. 1) passing through point  $P$  and parallel to the sheet width which divides the single-layered GNR into two distinctly vibrating regions. We note that the frequency of oscillation changes by fixing an interior atom.

The mode localization in [15,16] has been defined by using a parameter  $\beta$  that equals the ratio of the strain energy of deformation in one of the two regions divided by the strain energy of deformation of the entire region. For region  $\Omega_1$ , the parameter  $\beta_1$  is calculated from the equation

$$\beta_1 = \frac{\sum_{\Omega_1} \Delta U}{\sum_{\Omega} \Delta U}, \quad (2)$$

where  $\Omega = \Omega_1 \cup \Omega_2$ . Here the potential energy of an atom equals the difference in its potential energies in the deformed (an extremum of a mode) and the undeformed (mean) configurations of the single-layered GNR. Of course,  $\beta_2 = 1 - \beta_1$ . For continuum structures studied in [15,16] one finds the modal strain energy to compute  $\beta$  by assuming that the undeformed configuration has zero potential energy. Here we use ANALYZE subroutine of TINKER [20] to compute the potential energy of the deformed single-layered GNR. The distribution of  $\beta_1$  for the first forty out-of-plane bending modes of the single-layered GNR without an interior clamped atom is shown in Fig. 3(a). It is found that for most modes  $\beta_1 \approx 0.2$  which equals the ratio of the surface area of the region  $\Omega_1$  to that of the domain  $\Omega$  of the single-layered GNR. However, when the interior atom at  $P$  (cf. Fig. 1) is also fixed then modes get localized. For this case modes with  $\beta_1 > 0.2$  get localized in region  $\Omega_1$  and those with  $\beta_1 < 0.2$  get localized in region  $\Omega_2$ . The distribution of  $\beta_1$  for a single-layered GNR with a fixed interior atom is shown in Fig. 3(b). It is clear that 13 modes with  $\beta_1 \sim 0$  are strongly localized in region  $\Omega_2$ . Similarly, 2 modes with  $\beta_1 \sim 0.9$  (or  $\beta_2 \sim 0.1$ ) are strongly localized in  $\Omega_1$ . Furthermore, a value of  $\beta_1$  close to 0.2 or  $\beta_2$  close to 0.8 indicates moderate mode localization whereas a value of  $\beta_1 = 0.2$  or  $\beta_2 = 0.8$  indicates no mode localization.

In order to quantify the dependence of mode localization on the aspect ratio ( $L/W$ ) of a single-layered GNR we define the connection coefficient [15,16],  $C = \frac{1}{S} \sum_{j=1}^S \min(\beta_1, (1 - \beta_1))_j$ , where  $S$  equals the number of out-of-plane modes of interest. In the present study we have used  $S = 10$ . The variation in the value of  $C$  with  $L/W$  is shown in Fig. 4 for both the pristine single-layered GNR and that with a fixed interior atom at ( $L/5, W/2$ ). For the latter case with increasing aspect ratio (keeping the width  $W$  constant) the two regions become more disconnected which implies that modes are either localized in region  $\Omega_1$  or in  $\Omega_2$ . However, for the former case the value of  $C$  is found to oscillate around 0.2. This is similar to that found by Filoche and Mayboroda [15] and Sharma et al. [16] for vibration of CCCC plates/laminates with an interior fixed point.

In our studies on single-layered GNRs we have found that the phenomenon of mode localization is independent of the position of the fixed atom. However, the degree of mode localization varies. For the sake of brevity these results are omitted.

### 3.2. Multi-layered GNRs

In practice it may be difficult and uneconomical to peel-off a pristine single-layered GNR from bulk graphite. This motivates us to study vibrations of multi-layered GNRs [7,21] with and without an interior atom fixed only on one of the outermost layers. In our simulations for one- through five-layered pristine GNRs subjected to CCCC boundary condition we have found that the vibration characteristics, i.e., the bending modes (BMs) and the frequencies of a single layer govern the vibration characteristics of the entire stack. From frequencies listed in the top set of Table 1 we see that for two- to five-layered GNRs the frequencies of the 1st through the 4th bending mode differ from the corresponding modes of the

single-layered GNR by  $\leq 2.5\%$ . This is counter-intuitive in the sense that increasing the number of layers of the same material (i.e., the thickness of the GNR) the bending stiffness divided by the areal density (i.e., mass density/volume multiplied by the GNR thickness) is almost unchanged and hence very little change in the frequency occurs. Furthermore, this suggests that the shear deformation, if any, plays a negligible role if one were to model multi-layered GNRs as continuum plates to find the first few bending mode frequencies. We note that studying vibrations of multi-layered GNRs with the Mindlin plate theory requires more work [22,23] than that with the Kirchhoff plate theory in which effects of shear deformations are neglected.

When an interior atom on an outermost layer of a multi-layered GNR was fixed we found that the mode localization in this outermost layer of the GNR induced localization in the remaining layers. This new phenomenon of cooperative mode localization for a two-layered GNR is exhibited in Fig. 5. The quantification of mode localization in multi-layered GNRs requires a new parameter because the parameter  $\beta_1$  [15] defined above does not yield a unique value for the two extreme configurations of a particular mode. This is due to the fact that the fixed interior atom in an outermost layer leads to asymmetric out-of-plane deformations in the two extreme

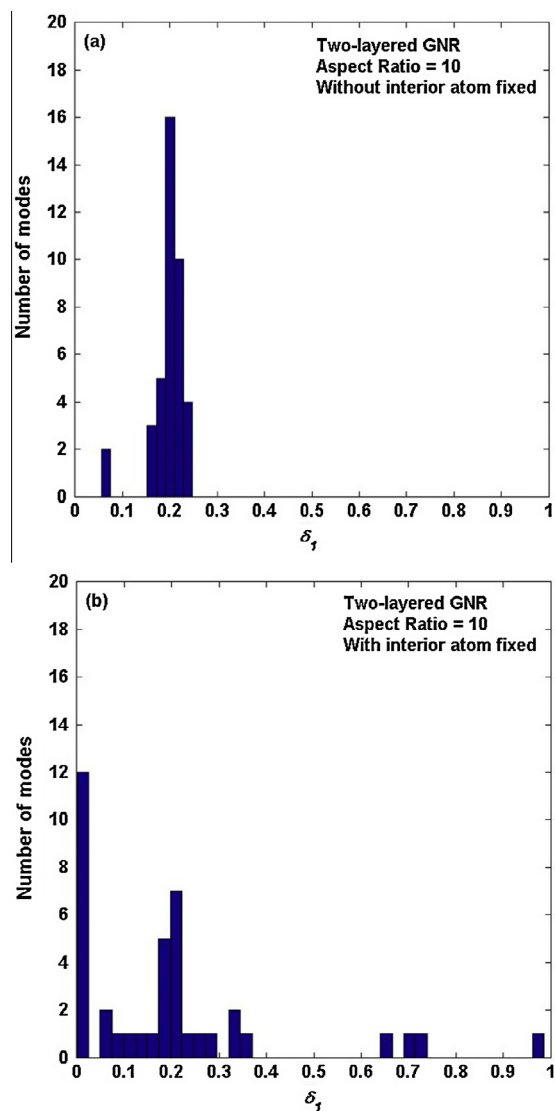


Fig. 6. Distribution of the mode localization parameter  $\delta_1$  computed over the first 40 out-of-plane modes for two-layered GNR (a) without, and (b) with interior fixed atom at  $P$  (cf. Fig. 1).

configurations of a mode (cf. insets of Fig. 5(a) and (b)). Hence the computed potential energy of atoms in region  $\Omega_1$  is different for the two configurations. This asymmetry leads to different values of localization parameter  $\beta$  for the two extreme configurations. However, the total change in the potential energy is the same in both extreme positions. Accordingly, we introduce a new parameter  $\delta_1$  defined by

$$\delta_1 = \frac{\sum_{\Omega_1} (\Delta x_i^2 + \Delta y_i^2 + \Delta z_i^2)}{\sum_{\Omega} (\Delta x_i^2 + \Delta y_i^2 + \Delta z_i^2)}, \quad (3)$$

where  $\Delta x_i$ ,  $\Delta y_i$ , and  $\Delta z_i$  are displacements of the  $i$ th atom in the  $x$ -, the  $y$ -, and the  $z$ -directions, respectively, from the initial equilibrated configuration to that of extreme position for the mode of vibration being considered. The region  $\Omega_1$  is defined in the same way as for a single-layered GNR but it now includes atoms in all layers on the left of the plane perpendicular to the plane of GNR passing through  $AB$  (cf. Fig. 1), and  $\Omega$  has all atoms in all layers. Whereas values of  $\beta$  for the two extreme configurations of a mode are different, those of  $\delta_1$  are the same.

The distribution of  $\delta_1$  with and without a fixed interior atom in a layer computed for the first forty out-of-plane modes for a two-layered GNR is exhibited in Fig. 6. As for a single-layered GNR with no interior atom clamped we see that for most modes  $\delta_1 \approx 0.2$ .

After fixing an interior atom in a layer, a significant number of modes have  $\delta_1 \approx 0$  implying that the two-layered GNR has modes silent in region  $\Omega_1$ . Additionally, out of the forty out-of-plane modes studied here it is found that there is a mode with  $\delta_1 = 0.9862$  in the two-layered GNR which gets localized in  $\Omega_1$ . This mode is shown in Fig. 5.

In Table 1 we have compared frequencies of the first four bending modes (BMs) for pristine single- and multi-layered GNRs (top set) with those computed for the single- and the multi-layered GNRs (middle set) having an interior atom fixed on an outermost layer. In general clamping an atom increases the frequency for a given mode number in the spectrum over that of the pristine single- or multi-layered GNR. For the first BM the increase in the value of the frequency for the single- and the multi-layered GNRs studied here is less than 1%. For higher modes the percent change in the frequency is found to be more, for example in the 4th BM the value of frequencies for all the single- and the multi-layered GNRs is found to increase by  $\sim 6\%$  after fixing an atom on an outermost layer. In Fig. 7 we show *cooperative mode localization* in one- to five-layered GNRs for (5, 1) mode. In this particular mode of vibration with increasing number of layers the value of  $\delta_1$  is found to increase indicating almost negligible out-of-plane deflections in region  $\Omega_2$ . Since the fixed atom is at  $L/5$  (a node point for the fifth mode (5, 1) of the pristine GNRs) the frequency of vibration for all

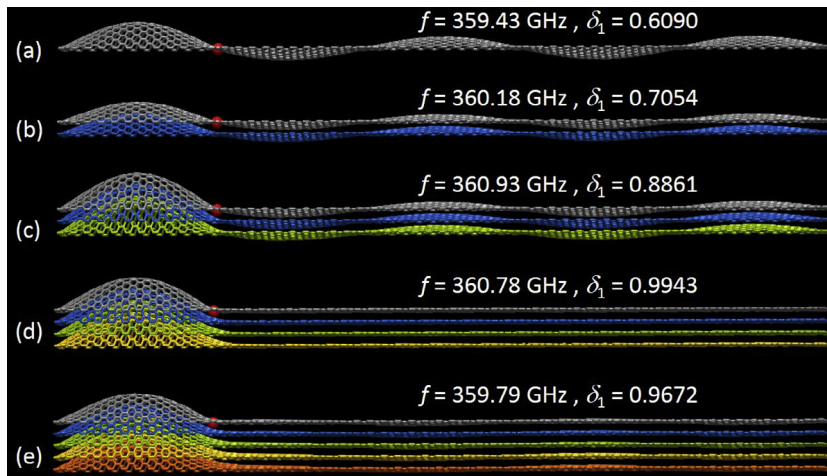


**Fig. 7.** Cooperative mode localization in multi-layered GNR due to a fixed interior atom (shown as red dot) on the topmost layer (gray colored). With increasing number of layers mode localization is found to be stronger as evidenced by the value of the  $\delta_1$  - parameter for each case. (For interpretation of the references to color in this figure legend, the reader is referred to the web version of this article.)

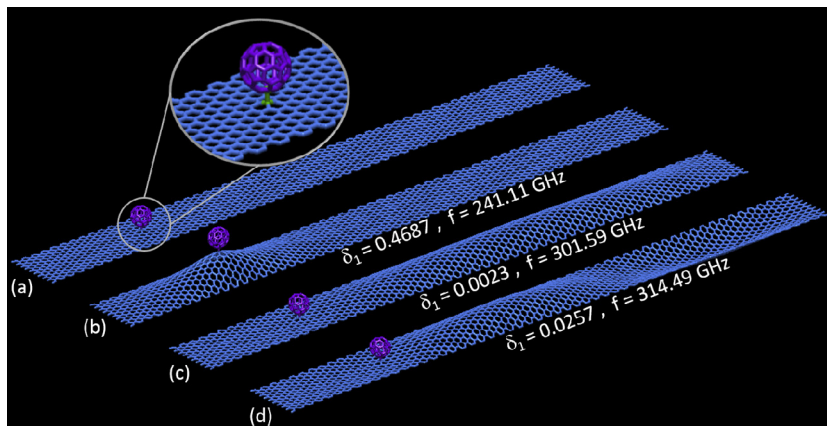


**Fig. 8.** Mode localization in GNR due to attached mass: (a) clamped-clamped-clamped-clamped GNR with  $C_{60}$  molecule covalently bonded at  $P$  (see Fig. 1), (b) the first mode, (c) and (d) show the localized modes (1, 1) and (2, 1), respectively.

**Table 2**

Frequencies (in GHz) of different bending modes (BMs) of pristine GNR, GNR with attached family of bucky-balls at ( $L/5, W/2$ ), and GNR with a fixed interior atom at ( $L/5, W/2$ ) computed from MM simulations. For all configurations GNRs are subjected to CCCC boundary condition. Dimensions of GNR;  $L = 227.77$  Å and  $W = 20.94$  Å. Number of C-atoms in GNR = 2148. Mode shape corresponding to Mode 1 vibrations of the GNR with a bucky-ball covalently bonded to an interior atom is shown in Fig. 8b.

Molecular structure	Mode 1	BM 1	BM 2
Pristine GNR	299.52 <sup>a</sup>	307.05 <sup>a</sup>	319.56 <sup>a</sup>
GNR + C <sub>30</sub>	273.51	301.62	313.86
GNR + C <sub>60</sub>	241.11	301.59	314.49
GNR + C <sub>90</sub>	218.82	301.71	314.61
GNR + C <sub>100</sub>	215.67	301.02	314.04
GNR + C <sub>180</sub>	179.85	301.50	313.86
GNR + C <sub>240</sub>	170.19	301.20	313.80
GNR with fixed atom at $P$	–	301.26	313.44

<sup>a</sup> Marked numbers are to be read as frequencies of 1st, 2nd and 3rd modes in increasing order for pristine GNR.

the cases is found to be nearly the same, however, mode shapes are different. From these results it can be concluded that the cooperative mode localization is inevitable in a multi-layered GNR if an outermost layer has a localized mode of vibration.

#### 4. Mode localization due to attached foreign molecule

In this section we investigate the phenomenon of mode localization due to a bucky-ball covalently bonded to an interior atom in CCCC and CFCF single-layered GNRs and to an interior atom of an outermost layer of multi-layered CCCC GNRs. The work is

motivated by the work in the area of NEMSs [5,7–9,24] in which GNRs are suspended over a trench.

#### 4.1. Single-layered GNRs

##### 4.1.1. CCCC boundary condition

We use the geometry shown in Fig. 1. Moreover, the  $sp^3$  hybridized atom located at  $P$  (cf. Fig. 1) is covalently bonded to an atom of a bucky-ball as shown in the inset of Fig. 8(a). The minimum potential energy configuration of this combined system is found by using the method described in Section 2. Similar to the studies of continuum plates by Sharma et al. [16] attaching a mass on a single-layered GNR also results in localization of modes of vibration as shown in Fig. 8(b–d). We have studied mode localization when an atom of the C<sub>30</sub>, C<sub>60</sub>, C<sub>90</sub>, C<sub>100</sub>, C<sub>180</sub>, and C<sub>240</sub> molecules is covalently bonded to the atom at  $P$ . We note that modes of vibration of these GNRs are not necessarily of the type  $(m, n)$  mentioned above. In all these cases the frequency of the first mode (Mode 1) corresponding to Fig. 8(b) is found to decrease with an increase in the mass (cf. Table 2) of the attached bucky-ball. This agrees with the fundamentals of the theory of vibration and is exploited in mass sensors [3,11,25]. For the reason discussed in Section 3.2 to quantify mode localization we use the parameter  $\delta_1$  defined by Eq. (3). Furthermore, for localized first and second BMs depicted in Fig. 8(c) and (d), respectively, the value of the parameter  $\delta_1$  is found to be very small. Thus, the effective length of the GNR could be considered to be reduced by  $L/5$ . Hence for these modes for different values of the added mass the frequencies are found to be approximately the same as those listed in Table 2. This also holds when an atom at  $P$  is fixed (cf. the last row of Table 2).

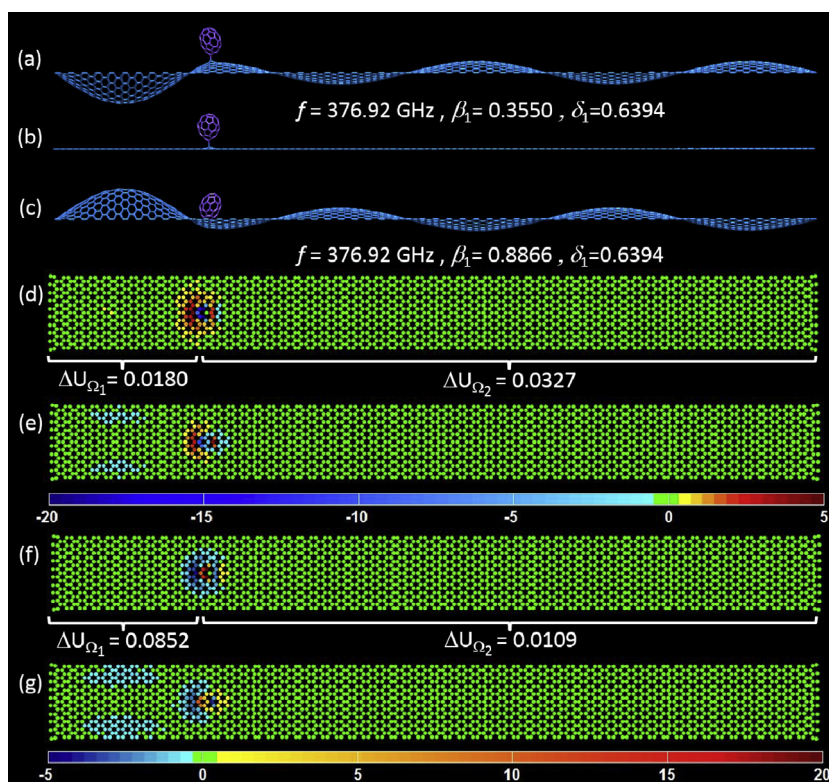


**Fig. 9.** Two extreme configurations (a) and (c) of the mode of vibration of a GNR with the C60 bucky-ball covalently bonded to an interior atom of a GNR shown in (b). Fringe plots of the total energy and van der Waal energy of deformation for configuration in (a) are shown in (d) and (e), and for (c) in (f) and (g), respectively. Color bar for (d) and (e) is shown below (e) and that for (f) and (g) is shown below (g). Both have units of cal/mol. The values of  $\beta_1$  for both the cases are computed by substituting relevant values of  $\Delta U$  in Eq. (2). (For interpretation of the references to color in this figure legend, the reader is referred to the web version of this article.)

We have displayed in Fig. 9 extreme positions of a mode of vibration of a GNR with the  $C_{60}$  bucky-ball covalently bonded to an interior atom and fringe plots of the potential energy of deformation ( $\Delta U$ ). Energy plots shown in Fig. 9(d) and (f) are obtained after subtracting the total energy of an atom in configuration shown in Fig. 9(b) from those in configurations of Fig. 9(a) and (c), respectively. It is found that the difference in the total potential energy in the energy plots in most of the region is positive. However, the region close to bucky ball has this difference negative.

In order to better understand this we have used the ANALYZE module of TINKER to compute values of each component of the potential energy given in Eq. (1) for configurations of Fig. 9(a) and (c). In Fig. 9(e) and (g) plots of only the van der Waals energy of deformation for these extreme configurations of the GNR and the bucky-ball system is shown. It is found from these plots that the energy landscape of atoms in the GNR near the bucky-ball is approximately the same for both the total potential energy and the van der Waals energy of deformation for each extreme configuration of the GNR and the bucky-ball system. Therefore, we conclude that the significant contribution to the negative energy of deformation is due to the van der Waals interaction between the bucky-ball and the GNR. The negative values of the energy of deformation for GNR are also found to be from the bond-stretch, the angle-bend, the stretch-bend, the out-of-plane bend, the torsional, and the stretch-torsional deformations but these are insignificant compared to van der Waals energy and hence are not shown here. Further, the components of the energy for different configurations of GNR and bucky ball combined are tabulated in Table 5. It is found that the total difference in the energy for the entire GNR and the bucky-ball system is positive and mostly due to van der Waals interactions. The negative values of the energy in Fig. 9(d) and (f) are for atoms only in the small neighborhood of the bucky-ball.

The asymmetry in the two extreme configurations of a vibratory mode results in a non-unique value of the parameter  $\beta_1$ . Hence, we use the parameter  $\delta_1$  to quantify mode localization. Histograms plotted in Fig. 10 show the degree of mode localization for the first forty out-of-plane modes in a single- and a two-layered graphene sheet when a  $C_{180}$  molecule is attached to the atom at  $P$  (cf. Fig. 1). More number of modes (out of the first 20) is localized in region  $\Omega_2$  for the single-layered GNR than those in the two-layered GNR. This is because the two-layered GNR is stiffer than the single-layered GNR, therefore, the development of standing waves in region  $\Omega_1$  is possible only at very high frequency except when the atom at  $P$  is on the nodal line of vibrating pristine GNR. We note that for pristine single- and multi-layered GNRs the histograms will have most modes clustered around  $\delta_1 = 0.2$ , similar to that shown in Figs. 3(a) and 6(a), respectively.

#### 4.1.2. CFCF boundary condition

In this sub-section, using MM, we first study vibrations of an un-stretched and stretched rectangular pristine GNR having aspect ratio (AR, length/width) of  $\sim 10$ . We note that in devices using single-layered GNRs there is a built-in tension due to van der Waals interaction between the edges of a suspended single-layered GNR and the substrate [7,9,10,26]. The procedure to compute mode shapes and frequencies of vibrations of stretched single-layered GNRs using MM simulations is as follows. Atoms on the small edge ( $x = 0$ ) are fixed and those on the other small edge ( $x = L$ ) are prescribed incremental displacement  $\Delta$  such that these atoms occupy new positions ( $x + \Delta, y, 0$ ). Atoms on the two edges ( $x = 0, L$ ) are then held stationary. The minimum potential energy configuration of a single-layered GNR for incremental values of  $\Delta$  is found to within rms gradient of 0.001 kcal/mol/Å, and the VIBRATE subroutine is used to find frequencies of vibration for different modes. The values of the frequencies of the first four BMs and the first two

torsional modes (TMs) for various values of  $\Delta$  are given in Table 3. These suggest that with increase in  $\Delta$  the higher bending mode frequencies are found to be nearly integer multiple of the lowest BM frequency. This indicates that at high value of  $\Delta$  the membrane strain energy dominates over the bending strain energy and hence the single-layered GNR behaves as a membrane or a continuum string. We recall that the AR of the single-layered GNR studied is  $\sim 10$ . However, if one were to simulate or experiment with a pre-stretched single-layered GNR of AR  $\sim 1$  then the membrane model would be more appropriate. Furthermore, the variation with  $\Delta$  of the values of the BM frequencies of the single-layered GNR is quadratic which also holds for frequencies of a continuum string [27] with initial stretch  $\Delta$ . Frequencies of the continuum models are discussed in Section 5.

We now study vibrations of the single-layered GNR with a  $C_{180}$  molecule attached at  $P$  (cf. Fig. 1). Frequencies of vibration for the first four BMs and the first two TMs for various value of the initial stretch  $\Delta$  are listed in Table 4. For  $\Delta \geq 0.4$  Å frequencies of all modes studied here are found to be lower than those for the untreated prestretched single-layered GNR (cf. Table 3). This is similar to that for the unstretched CCCC single- or multi-layered

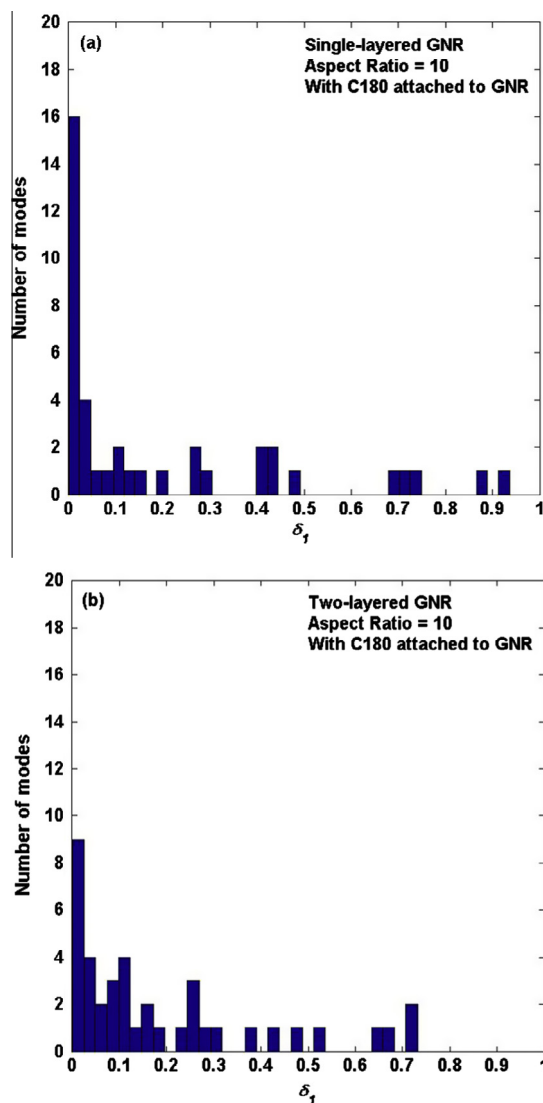


Fig. 10. Distribution of the mode localization parameter  $\delta_1$  computed over first 40 out-of-plane modes for (a) single- and (b) double-layered GNRs when  $C_{180}$  molecule is covalently bonded to the atom at  $P$  (cf. Fig. 1).

GNRs for which results are given in Table 1. In the MM simulations for  $\Delta = 0.8 \text{ \AA}$  we could not locate the 4th BM. Two BMs and one TM of vibration for the unstretched single-layered GNR with attached  $C_{180}$  molecule are shown in Fig. 11. The mode depicted in Fig. 12(c) is very interesting because in this mode of vibration the material in region  $\Omega_1$  undergoes bending while that in  $\Omega_2$  torsional oscillations. In this case indeed the attached  $C_{180}$  molecule divides the single-layered GNR into two independently vibrating regions. In Fig. 12 two BMs and a TM are shown for the single-layered GNR with  $\Delta = 1 \text{ \AA}$ . For this case we did not find localized BM in the spectrum before the appearance of the localized TM as shown in Fig. 12(c). It is possible that for the stretched single-layered GNR localized BMs are shifted towards the far end of the spectrum.

## 4.2. Multi-layered GNRs

When a  $C_{180}$  molecule is covalently bonded to an atom of an outermost layer of a multi-layered GNR, we get cooperative mode localization. Frequencies of the first five BMs for one- to five-layered GNR with  $C_{180}$  molecule covalently bonded to an atom at point  $P$  (cf. Fig. 1) of an outermost layer are listed in the last set of Table 1. Unlike the situation when an atom at  $P$  on an outermost layer is fixed in this case we get an additional mode of vibration for

GNRs. The frequency of this mode is lower than that of the 1st BM of pristine GNRs. For a five-layered GNR this mode is shown in Fig. 13. Only after this mode the localized BMs are found in the spectrum. As mentioned before the mode localization reduces the effective length of the GNR and hence the frequencies of oscillations (cf. Table 1) of the 1st BM to the 4th BM in the last set are almost the same as those for the middle set.

## 5. Continuum models

### 5.1. String model for single-layered GNRs subjected to CFCF boundary condition

The frequency  $f_n$  (in Hz) of a prestretched string made of a linear elastic, isotropic and homogeneous material is proportional to the square root of the pretension  $T_0$ . For a stretched single-layered GNR, the expression for  $f_n$  in terms of  $\Delta$  can be written as [27]

$$f_n = \frac{n}{2L} \sqrt{\frac{\Delta W(Eh)}{Nm_c}}, \quad n = 1, 2, \dots \quad (4)$$

In Eq. (4)  $L$ ,  $W$ ,  $h$ , and  $E$  are the length, the width, the thickness, and Young's modulus of the single-layered GNR, respectively, and  $N$  and  $m_c$  are the total number of C-atoms in the single-layered GNR and

**Table 3**

Comparison of frequencies (in GHz) of bending and torsional modes of a GNR with CFCF boundary condition, obtained from MM simulations, string model (SM), and the finite element method (FEM) for different values of the initial stretch. Dimensions of GNR:  $L = 227.77 \text{ \AA}$  and  $W = 20.94 \text{ \AA}$ . No. of C-atoms in GNR = 2148. Material properties of equivalent continuum structures are taken from [2]. N.A. stands for not applicable.

Mode	$\Delta = 0 \text{ \AA}$			$\Delta = 0.2 \text{ \AA}$			$\Delta = 0.4 \text{ \AA}$			$\Delta = 0.6 \text{ \AA}$			$\Delta = 0.8 \text{ \AA}$			$\Delta = 1 \text{ \AA}$		
	MM	FEM		MM	SM	FEM	MM	SM	FEM	MM	SM	FEM	MM	SM	FEM	MM	SM	FEM
BM 1	2.46	3.87		12.72	12.66	13.98	17.85	17.91	19.14	21.81	21.93	23.13	25.11	25.32	26.49	28.05	28.32	29.61
BM 2	9.78	10.68		26.94	25.32	28.68	36.75	35.82	38.79	44.46	43.86	46.68	50.97	50.64	53.40	56.73	56.64	59.28
BM 3	21.90	20.91		43.53	37.98	44.79	57.51	53.73	59.46	68.64	65.79	71.07	78.15	75.99	80.94	86.58	84.96	89.70
BM 4	38.94	34.59		63.48	50.64	62.85	80.85	71.64	81.60	95.01	87.72	96.63	107.25	101.31	81.66	118.20	113.28	121.08
TM 1	35.40	26.97		37.59	N.A.	29.91	39.48	N.A.	32.55	41.31	N.A.	34.98	43.02	N.A.	37.26	44.64	N.A.	39.42
TM 2	71.70	54.33		75.78	N.A.	60.12	79.53	N.A.	65.37	83.10	N.A.	70.23	86.52	N.A.	74.79	89.73	N.A.	79.05

**Table 4**

Comparison of frequencies (in GHz) of bending and torsion modes of a GNR with CFCF boundary condition, with attached  $C_{180}$  molecule at  $(L/5, W/2)$ , obtained from MM simulations, string model (SM), and the finite element method (FEM) for different values of the initial stretch. Dimensions of GNR:  $L = 227.77 \text{ \AA}$  and  $W = 20.94 \text{ \AA}$ . Number of C-atoms in GNR = 2148. Material properties of equivalent continuum structures are taken from [2]. N.A. stands for not applicable. For  $\Delta = 0.8 \text{ \AA}$  BM 4 is not found in MM simulations.

Mode	$\Delta = 0 \text{ \AA}$			$\Delta = 0.2 \text{ \AA}$			$\Delta = 0.4 \text{ \AA}$			$\Delta = 0.6 \text{ \AA}$			$\Delta = 0.8 \text{ \AA}$			$\Delta = 1 \text{ \AA}$		
	MM	FEM		MM	SM	FEM	MM	SM	FEM									
BM 1	4.11	3.81		12.96	12.27	13.62	16.23	17.34	18.63	18.24	21.27	22.5	25.38	24.57	25.77	27.39	27.45	28.65
BM 2	10.29	10.05		25.02	23.46	26.73	33.33	33.18	36.06	39.75	40.62	43.32	46.74	46.92	49.50	52.62	52.44	54.93
BM 3	21.81	19.35		34.68	35.76	41.79	53.28	50.55	55.59	63.03	61.92	66.45	72.57	71.49	80.25	78.33	79.95	83.91
BM 4	37.62	32.97		59.25	49.59	60.69	62.07	70.11	65.37	95.31	85.89	93.72	-	99.18	106.35	117.03	110.88	117.57
TM 1	32.79	26.97		40.65	N.A.	29.91	35.31	N.A.	32.55	36.69	N.A.	34.98	39.21	N.A.	37.26	40.38	N.A.	39.42
TM 2	58.02	54.33		60.15	N.A.	60.12	71.55	N.A.	65.37	64.11	N.A.	70.23	66.21	N.A.	74.79	67.98	N.A.	79.05

**Table 5**

Energy components of GNR and buck-ball combined for configurations shown in Fig. 9.

Energy components	Energy corresponding to Fig. 9(a) (kcal/mol) (I)	Energy corresponding to Fig. 9(b) (kcal/mol) (II)	Energy corresponding to Fig. 9(c) (kcal/mol) (III)	(I)–(II) (kcal/mol)	(III)–(II) (kcal/mol)
Bond-stretch	307.74	307.35	307.62	0.39	0.27
Angle bend	505.31	505.33	505.34	–0.02	0.01
Stretch–bend	–114.00	–113.94	–113.96	–0.05	–0.02
Angle–angle	–32.47	–32.47	–32.47	0.00	0.00
Out-of-plane bend	85.85	85.86	85.88	–0.01	0.02
Torsional	–3353.99	–3354.06	–3353.98	0.06	0.08
Stretch–torsion	–1.81	–1.80	–1.79	–0.01	0.01
van der Waals	3373.13	3150.91	3373.12	222.22	222.21
Total	552.22	774.80	774.80	222.58	222.58

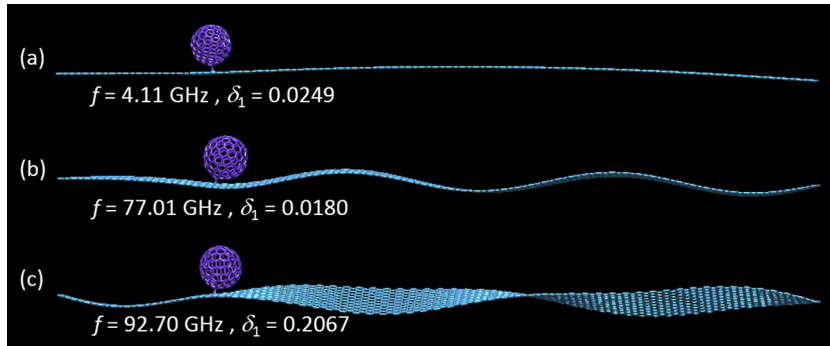


**Fig. 11.** Localized modes of vibration of an un-stretched GNR with bucky-ball  $C_{180}$  attached to an interior atom. Modes in (a) and (b) are the bending modes. The mode of vibration in (c) shows bending oscillation on the left and torsion oscillation on the right of  $C_{180}$  molecule.

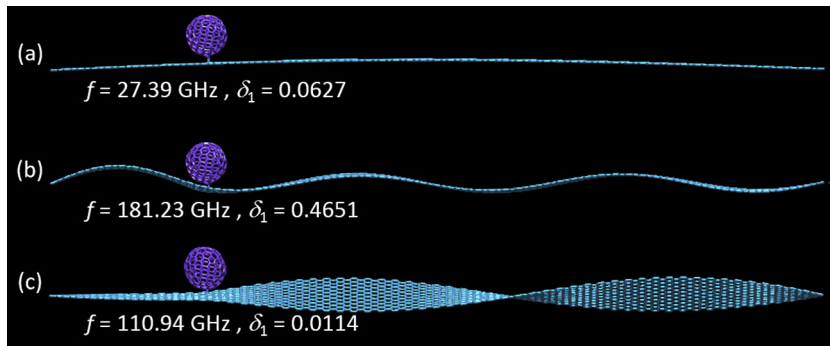


**Fig. 12.** Modes of vibration of 1 Å stretched GNR with bucky-ball  $C_{180}$  bonded to an interior atom. Modes in (a) and (b) are the bending modes. The mode in (c) shows negligible oscillations on the left and torsion oscillations on the right of the atom to which  $C_{180}$  molecule is covalently bonded.

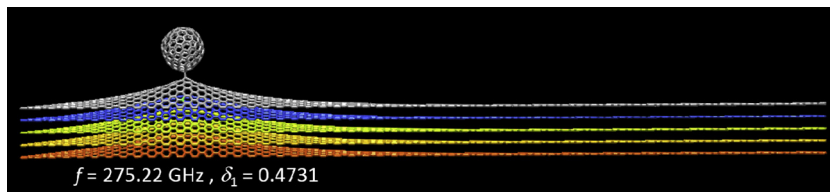


**Fig. 13.** Cooperative mode localization in the 5-layered GNR due to  $C_{180}$  bucky-ball covalently bonded to an atom on the outermost layer. The slope discontinuity in the eigenmodes of the outermost layer is not present in the layers below it.

the mass of a C-atom, respectively. The quantity  $Eh$  is the basal plane stiffness of the single-layered GNR and its value of 340 N/m is taken from our previous work [2] which agrees with the experimental value reported in [6]. Note that for  $\Delta = 0$  the string model is not valid. For different values of  $\Delta \neq 0$  values of frequencies for BMs computed from the string model (SM), i.e., Eq. (4), listed in Table 3 agree well with those found from our MM simulations. However, the SM does not give TMs of vibrations found in the MM simulations.

We investigate below if the SM with a concentrated mass attached to an interior point can predict results close to those given by the MM simulations.

#### 5.1.1. Frequency equation of equivalent string-mass system

Consider a uniform, homogeneous string held taut between two fixed ends, as shown in Fig. 14, having uniform tension  $T_0$ , mass density/volume  $\rho$ , cross sectional area  $A$ , length  $L$ , and a concentrated mass  $m$  attached to it at distance  $a$  from the left end. The governing equation of motion obtained using Newton's 2nd law and the associated boundary conditions for the system are [30]

$$[\rho A + m\delta(x-a)]w_{,tt} - T_0 w_{,xx} = 0; \quad w(0) = w(L) = 0. \quad (5)$$

Using the method of separation of variables, we set  $w(x, t) = W_0\phi(x)e^{ipt}$ , where  $W_0$  is the amplitude of vibration,  $\phi(x)$  is the configuration of the string-mass system and  $p$  is the frequency of vibration. Substitution for  $w(x, t)$  in Eq. (5) yields

$$p^2[\rho A + m\delta(x-a)]\phi(x) + T_0\phi''(x) = 0; \quad \phi(0) = \phi(L) = 0. \quad (6)$$

The Laplace transform of Eq. (6) reduces it to the following algebraic equation

$$T_0[s^2\bar{\phi}(s) - s\phi(0) - \phi'(0)] + p^2\rho A\bar{\phi}(s) + p^2m\phi(a)e^{-sa}\Theta(a) = 0, \quad (7)$$

where  $s$  is the Laplace variable,  $\bar{\phi}(s)$  is the Laplace transform of  $\phi(x)$ , and  $\Theta(\cdot)$  is the Heaviside step function. By substituting  $\phi(0) = 0$  in

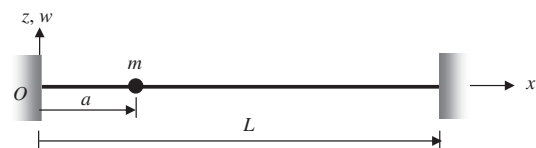


**Fig. 14.** Schematic diagram of a string with a concentrated mass  $m$  at an arbitrary distance  $a$  from the left edge  $O$ . The transverse displacement of a material particle of the string along the  $z$ -axis is  $w$ .

Eq. (7) that follows from the boundary conditions listed in Eq. (6), and rearranging terms we obtain

$$\bar{\phi}(s) = \frac{\phi'(0)}{s^2 + \beta^2} - \left( \frac{p^2 m \phi(a) \Theta(a)}{T_0} \right) \left( \frac{e^{-as}}{s^2 + \beta^2} \right), \quad (8)$$

where  $\beta^2 = p^2 \rho A / T_0$ . Taking the inverse Laplace transformation of Eq. (8) we get

$$\phi(x) = \phi'(0) \frac{\sin \beta x}{\beta} - \left( \frac{p^2 m \phi(a) \Theta(a)}{T_0} \right) \left( \frac{\Theta(x-a) \sin((x-a)\beta)}{\beta} \right). \quad (9)$$

In Eq. (9) the unknown  $\phi'(0)$  can be found using the second of the boundary conditions given in Eq. (6). We thus get

$$\phi(x) = \left( \frac{p^2 m \phi(a) \Theta(a)}{\beta T_0} \right) \left( \frac{\Theta(L-a) \sin((L-a)\beta) \sin \beta x - \Theta(x-a) \sin((x-a)\beta) \sin \beta L}{\sin \beta L} \right). \quad (10)$$

Setting  $x = a$ , and using the definition of the Heaviside step function gives

$$\phi(a) \left[ 1 - \frac{p^2 m}{\beta T_0} \left( \frac{\sin((L-a)\beta) \sin \beta a}{\sin \beta L} \right) \right] = 0. \quad (11)$$

Since  $\phi(a) = 0$  implies  $\phi(x) = 0$  from Eq. (10), we conclude from Eq. (11) that the term in brackets must vanish which is the frequency equation. Furthermore, using Hooke's law, the tension in the string is given by  $T_0 = KW\varepsilon$ , where  $K$ ,  $W$  and  $\varepsilon$  are the basal plane stiffness ( $Eh$ ), the width and the applied initial axial strain in the GNR, respectively. In particular, for  $a = L/5$  the frequency equation is

$$\frac{1}{p} \sqrt{\frac{M\xi}{m^2}} = \frac{\sin \left[ \frac{4p}{5} \sqrt{\frac{M}{\xi}} \right] \sin \left[ \frac{p}{5} \sqrt{\frac{M}{\xi}} \right]}{\sin \left[ p \sqrt{\frac{M}{\xi}} \right]}, \quad (12)$$

where  $M$  is the mass of the GNR, and  $\xi = KW\varepsilon/L$ . Roots of Eq. (12) are the natural frequencies of the system described by Eq. (5). For various values of  $\Delta$  these roots are found using MATHEMATICA [32]. Frequencies for the first four BMs are given in Table 4. As stated above, this model is not valid for  $\Delta = 0$  and TMs cannot be captured. Predictions from this model listed in Table 4 suggest that with an increase in the value of  $\Delta$  the difference in values of frequencies from Eq. (12) and the MM simulations decreases. We note that in [30,31] authors have given the frequency equation for the specific case of  $a = L/2$ .

## 5.2. Plate model for CFCF single-layered GNRs

In order to capture the TMs we model the single-layered GNR as a thin plate using Kirchhoff's plate theory [28], and use the finite element method (FEM) with the 8-node shell-93 element in ANSYS [29] to find frequencies for various values of  $\Delta$  considered in the MM simulations. The elastic and mass properties for the FE simulations are taken from our previous work [2]. A converged solution is obtained with the FE mesh  $10 \times 100$  (uniform elements along the width and the length, respectively) within 1% error in the frequencies of first 20 modes. The plate is prestretched by fixing all six degrees of freedom (three translational and three rotational) of nodes on one end while nodes on the other end are prescribed only the axial displacement keeping other five degrees-of-freedom restrained. Values of frequencies computed from the FE analysis are listed in Table 3. Even though the plate model is valid for the initial stretch  $\Delta = 0$  due to non-zero bending stiffness of the plate, for  $\Delta = 0$  frequencies of bending and torsional modes computed from the FE simulations appreciably differ from those derived from the MM simulations. With an increase in the value of  $\Delta$ , this

difference in the two sets of BM frequencies decreases more rapidly than that in the TB frequencies.

Frequencies of the first four BMs and the first two TMs of vibration of a single-layered GNR with the attached  $C_{180}$  molecule obtained from the FE simulations are listed in Table 4. We have used the same FE as that for the single-layered GNR but now we also use Mass-21 FE to simulate the  $C_{180}$  molecule, and place it at  $(L/5, W/2)$  on the mid-plane of the ECS of the single-layered GNR. The Mass-21 FE has only three translational degrees of freedom. In general, differences in the frequencies for all modes computed from the FEM are found to be larger than those when the  $C_{180}$  was not attached to the single-layered GNR. Possible reasons for this mismatch are: (i) placement of the mass element, and (ii) the van der Waals interaction between the  $C_{180}$  and the single-layered GNR could alter the local stiffness of the single-layered GNR that has not been considered in the FE model. For  $\Delta > 0.4 \text{ \AA}$ , frequencies of the bending and the torsion modes are found to decrease after attaching  $C_{180}$  molecule. Since the mass is attached at the bisector of the width of the FE model and is placed at the mid-plane frequencies of torsional modes are unaffected and are exactly the same as those for the case when no mass is attached to the ECS of the single-layered GNR (cf. Table 3).

A careful examination of the mode shapes computed from MM simulations and shown in Figs. 12 and 13 reveals that the buckyball deforms and oscillates. In order to simulate these, the FE model will require a flexible shell (an ECS of a buckyball) attached to the ECS of the single-layered GNR using flexible beam (an ECS of the bond between the buckyball and the single-layered GNR). Furthermore, the accuracy of the model can be increased by specifying interactions of the buckyball with the single-layered GNR using van der Waals springs. We leave this work for a future study. An attempt to consider these interactions was made by Batra and Sears [33] who developed continuum structures equivalent to a multi-walled carbon nanotube.

## 6. Conclusions

We have studied vibrations of single- and multi-layered graphene nano-ribbons (GNRs) using MM simulations and employing the MM3 potential. Two types of boundary conditions, all edges clamped (CCCC) and only two smaller edges clamped while the other two free (CFCF), are considered. In single- and multi-layered GNRs modes of vibrations are found to get localized due to either fixing an interior atom or attaching a (covalently bonded) buckyball to an interior atom. For both cases, in multi-layered GNRs mode localization in an outermost layer is found to induce localization in the remaining layers; we call this *cooperative mode localization*. A new parameter to quantify mode localization is defined for multi-layered GNRs with a fixed interior atom and for single- and multi-layered GNRs when a mass is attached to an interior atom. For CCCC single- and multi-layered GNRs, attaching a mass to an interior atom is found to reduce the frequency of vibrations of the first mode. Vibrations of CFCF single-layered GNRs with and without a mass attached to an interior atom are studied for different values of the initial stretch (0–1 Å) using MM and, continuum string-mass and thin plate models. With increasing value of the initial stretch the frequency of vibrations for bending and torsional modes is found to increase. For initial stretch of 1 Å values of the first four bending mode frequencies from the string-mass model are found to be closer to those obtained from the MM simulations than those computed from the thin plate model. With increasing value of initial stretch the difference in the frequencies computed from the FE model and those from MM simulations are found to decrease albeit not monotonically. In MM simulations for CFCF single-layered GNRs, the torsional modes are also found to get localized after attaching a  $C_{180}$  molecule to an interior atom.

It is noted here that even though we have studied single- and multi-layered GNRs with long armchair edges, due to the basal plane isotropy of GNRs [2,10], the findings of this research will remain unaffected if one were to use long zigzag edges. This study highlights the role of mode shapes and will be useful in designing efficient sensitive mass sensors and studying dynamics of single- and multi-layered GNRs suspended over a patterned surface.

### Appendix A. Supplementary material

Supplementary data associated with this article can be found, in the online version, at <http://dx.doi.org/10.1016/j.commatsci.2014.07.005>.

### References

- [1] S. Adhikari, R. Chowdhury, *Phys. E* 44 (2012) 1528–1534.
- [2] S.S. Gupta, R.C. Batra, *J. Comput. Theor. Nanosci.* 7 (2010) 2151–2164.
- [3] S.Y. Kim, H.S. Park, *Nanotechnology* 21 (2010). Art. no. 105710.
- [4] J.-W. Jiang, H.S. Park, T. Rabczuk, *Nanotechnology* 23 (2012) 475501.
- [5] O.K. Kwon, K.-S. Kim, J. Park, J.W. Kang, *Comput. Mater. Sci.* 67 (2013) 329–333.
- [6] N.L. Rangel, J.M. Seminario, *J. Chem. Phys.* 132 (2010). Art. no. 125102.
- [7] J.S. Bunch, A.M. van der Zande, S.S. Verbridge, I.W. Frank, D.M. Tanenbaum, J.M. Parpia, et al., *Science* 315 (2007) 490–493.
- [8] D. Garcia-Sanchez, A.M. van Der Zande, A.S. Paulo, B. Lassagne, P.L. Mceuen, A. Bachtold, *Nano Lett.* 8 (2008) 1399–1403.
- [9] S. Shivaraman, R.A. Barton, X. Yu, J. Alden, L. Herman, M. Chandrashekar, et al., *Nano Lett.* 9 (2009) 3100–3105.
- [10] C. Lee, X. Wei, J.W. Kysar, J. Hone, *Science* 321 (2008) 385–388.
- [11] C. Chen, S. Rosenblatt, K.I. Bolotin, W. Kalb, P. Kim, I. Kymissis, et al., *Nat. Nanotechnol.* 4 (2009) 861–867.
- [12] R.A. Barton, B. Ilic, A.M. van der Zande, W.S. Whitney, P.L. Mceuen, J.M. Parpia, et al., *Nano Lett.* 11 (2011) 1232–1236.
- [13] L. Wang, X. He, *J. Nanotechnol. Eng. Med.* 1 (2010) 041004.
- [14] T. Natsuki, J.-X. Shi, Q.-Q. Ni, *J. Appl. Phys.* 114 (2013). Art. no. 094307.
- [15] M. Filoche, S. Mayboroda, *Phys. Rev. Lett.* 103 (2009). Art. no. 254301.
- [16] D. Sharma, S.S. Gupta, R.C. Batra, *Compos. Struct.* 94 (2012) 2620–2631.
- [17] N. Allinger, Y.H. Yuh, J.-H. Lii, *J. Am. Chem. Soc.* 111 (1989) 8551–8566.
- [18] M.S. Rao, A.M. Richter, E. Bandow, S. Chase, B. Eklund, P.C. Williams, K.A. Fang, S. Subbaswamy, K.R. Menon, M. Thess, A. Smalley, R.E. Dresselhaus, G. Dresselhaus, *Science* 275 (1997) 187–191.
- [19] S.S. Gupta, R.C. Batra, *Comput. Mater. Sci.* 43 (2008) 715–723.
- [20] J.W. Ponder, *User's Guide, Tinker Molecular Modelling Software, Version 4, 2004.*
- [21] K.S. Novoselov, A.K. Geim, S.V. Morozov, D. Jiang, Y. Zhang, S.V. Dubonos, et al., *Science* 306 (2004) 666–669.
- [22] R. Ansari, S. Sahmani, B. Arash, *Phys. Lett. A* 375 (2010) 53–62.
- [23] A.R. Setoodeh, P. Malekzadeh, A.R. Vosoughi, *Proc. Int. Mech. Eng. C – J. MEC.* (2012) 1897–1906.
- [24] B. Arash, Q. Wang, *Comput. Mater. Sci.* 60 (2012) 245–249.
- [25] A. Sakhiae-Pour, M.T. Ahmadian, A. Vafai, *Solid State Commun.* 145 (2008) 168–172.
- [26] J. Atalaya, A. Isacson, J.M. Kinaret, *Nano Lett.* 8 (2008) 4196–4200.
- [27] L. Meirovitch, *Elements of Vibrations Analysis*, 2nd ed., Mc-Graw Hill Book Company, 1986.
- [28] S.P. Timoshenko, S. Woinowsky-Krieger, *Theory of Plates and Shells*, 2nd ed., Tata Mc-Graw Hill, 2010.
- [29] ANSYS 10.0, *User's Manual.*
- [30] Y. Chen, *J. Franklin Inst.* 276 (1963) 191–196.
- [31] B.J. Gómez, C.E. Repetto, C.R. Stia, R. Weltri, *Eur. J. Phys.* 28 (2007) 961–975.
- [32] Wolfram Research Inc., *Mathematica 8.0, Version 8.*, Wolfram Research, Inc., Champaign, Illinois, 2010.
- [33] R.C. Batra, A. Sears, *Int. J. Solids Struct.* 44 (2007) 7577–7596.